

RSC Advances



This is an *Accepted Manuscript*, which has been through the Royal Society of Chemistry peer review process and has been accepted for publication.

Accepted Manuscripts are published online shortly after acceptance, before technical editing, formatting and proof reading. Using this free service, authors can make their results available to the community, in citable form, before we publish the edited article. This *Accepted Manuscript* will be replaced by the edited, formatted and paginated article as soon as this is available.

You can find more information about *Accepted Manuscripts* in the [Information for Authors](#).

Please note that technical editing may introduce minor changes to the text and/or graphics, which may alter content. The journal's standard [Terms & Conditions](#) and the [Ethical guidelines](#) still apply. In no event shall the Royal Society of Chemistry be held responsible for any errors or omissions in this *Accepted Manuscript* or any consequences arising from the use of any information it contains.

Cite this: DOI: 10.1039/c0xx00000x

www.rsc.org/xxxxxx

ARTICLE TYPE

Novel cage-like α -Fe₂O₃/SnO₂ composite nanofibers by electrospinning for rapid gas sensing properties

Xin Li, Hang Zhang, Changhao Feng, Yanfeng Sun*, Jian Ma, Chong Wang and Geyu Lu*

Received (in XXX, XXX) Xth XXXXXXXXXX 20XX, Accepted Xth XXXXXXXXXX 20XX

DOI: 10.1039/b000000x

Novel α -Fe₂O₃/SnO₂ composite nanofibers were fabricated by a homotaxial electrospinning method. The cage-like nanofibers shows high selectivity to acetone as well as ultrafast response and recovery times within 3 s to 100 ppm acetone.

Recently, the detection of volatile organic compounds (VOCs) has become a very imperative task in many countries for environmental monitor, food inspection and medical diagnostics.¹ Especially in the factory, the excessive concentration of the VOCs may cause explosions, ambient air pollution and even human poisoning if not timely monitoring and feedback. Thus the research and development of quick-response metal oxides semiconductor chemical gas sensor has practical significance and prospect. Many semiconducting metal oxides have been used as sensor materials for VOCs detection. Among them, special attentions have been paid on SnO₂ and α -Fe₂O₃ due to their excellent gas sensing performances.²⁻¹⁰ Especially, the combination of them as well as the construction of their compositive nanostructures can further enhance the sensing characteristics to VOCs.¹¹⁻¹⁴ The key factors influencing sensitive nature of the sensing materials mainly include three aspects: the receptor function, the transducer function and the sensitive utilization of surface particles.¹⁵⁻¹⁷ Based on the above mechanism, we are committed to design a metal oxide gas sensing material with large specific surface area, good porous and uniformity in the meanwhile. Electrospinning technique can provide a simple and versatile route to prepare nanofibers with a large surface area to volume ratio, flexibility in surface functionalities, and heterostructure¹⁸. These nanofibers fabricated are very suitable for gas sensing application due to the small crystalline size, high surface area and high porosity. Inorganic metal oxides fabricated by electrospinning polymer solutions containing inorganic precursors with subsequent calcination at high temperature promising to give rise to high uniformity as sensor materials. The fibrous morphology can form a network of interconnected nanowires in which target gas can easily diffuse through large pores formed with nanowires. Simultaneously, small pores between the adjacent grains of metal oxide enable gas to get more active site to adsorption.

Jilin University, College of Electronic Science and Engineering, No. 6999, Qianjin Street, Jilin Province 130012, China. Fax: 86-431-85167808; Tel: 86-431-85167808; E-mail: syf@mail.jlu.edu.cn, luyg@mail.jlu.edu.cn

† Electronic Supplementary Information (ESI) available: Experimental section and images (Fig.S4) of the products prepared with different calcined temperatures and heating rates. See DOI: 10.1039/b000000x/

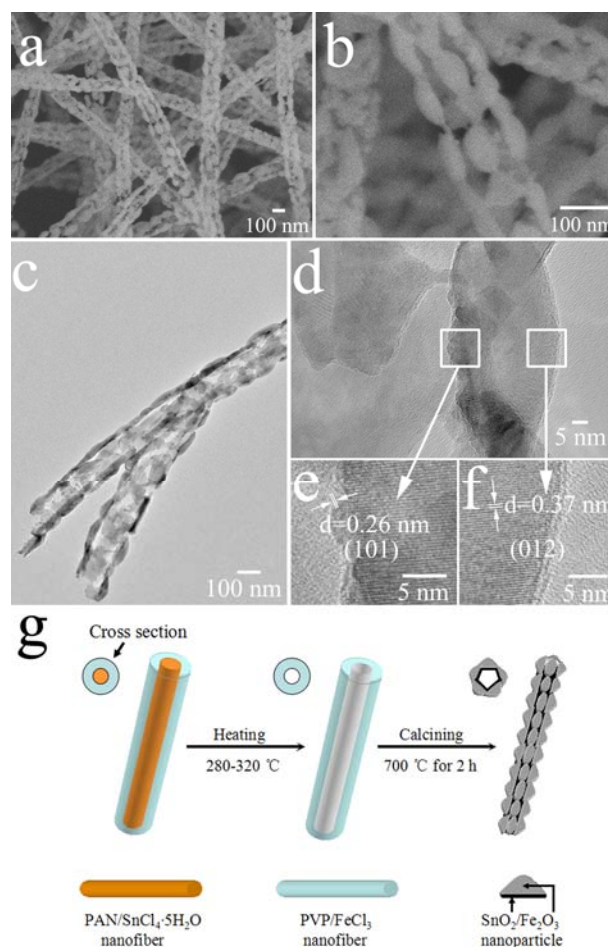


Fig.1 (a) FE-SEM picture of as spun α -Fe₂O₃/SnO₂ composite nanofibers, (b) magnified view of the hollow and porous nanofibers, (c and d) TEM and HRTEM images of the composite nanofibers, (e and f) HRTEM images recorded from the white frame marked in (d). (g) illustrate diagram of the possible formation process of α -Fe₂O₃/SnO₂ composite nanofibers through heat treatment procedure.

In a long time, studies have focus on the enhancement of gas response or gas responding kinetics due to the nanofibers morphology and less agglomerated network structure. However, research on the design of unique structure nanofibers with a purpose to improve certain aspects of the performance of gas sensors remains in the elementary stage. For example, when testing VOC gas such as acetone, the semiconductor oxide gas sensors generally show long response and recovery time. In this paper, we present an attempt to enhance response and recovery

kinetics of the metal oxides semiconductor gas sensor to VOCs by fabricating the composite nanofibers sensing materials with a novel morphology and structure. The materials with nanoscale and porous structure as gas sensors are supposed to not only provide a large number of channels for gas diffusion, but also possess significantly large surface areas for gas-sensing reactions.¹⁹ The synthesis process and experiment of raw materials are detailed introduced in supplementary information.

As shown in the FE-SEM images (Fig.1 a and b), the obtained samples which composed of drop-like nanoparticles exhibit the porous and hollow structure. It can be observed that the nanoparticles are well arranged and attach to each other forming chain cables, which construct the wall of the cage-like nanofibers. The size of each nanoparticle is about 30 nm. The average diameter of the α -Fe₂O₃/SnO₂ nanofibers is approximately 160 nm and the length is longer than 40 μ m. The transmission electron microscope (TEM) image (Fig. 1c) evidences the porous and hollow structure of the nanofibers, which is coherent with the observation in the FE-SEM images (Fig. 1a and b). The connection part of two nanoparticles in one chain cable is shown in Fig. 1d. The narrow neck connection of the two particles can be clearly observed, which is beneficial for obtain high response. The structure information was further characterized by HRTEM as shown in Fig. 1e and f, which corresponding to the white frames in Fig. 1d. The lattice spacings of 0.26 nm for the inside partial and 0.37 nm for the outside partial of the nanoparticle, respectively, correspond to the (101) plane of rutile SnO₂ and the (012) plane of rhombohedral α -Fe₂O₃. Fig.1 g schematically shows the construction core-shell structure of precursor before calcination and the formation process of α -Fe₂O₃/SnO₂ composite nanofibers. The sectional part of the nanofiber was shown in the upper left corner. Due to the incompatibility of PVP (polyvinylpyrrolidone) and PAN (polyacrylonitrile), the initial hierarchical solid structure has already been formed in precursor nanofibers.²⁰⁻²³ Core nanofibers comprising PAN and SnCl₄·5H₂O and shell nanofibers comprising PVP and FeCl₃ were electrospun from a dimethylformamide solution. According to the literatures,^{24,25} the degradation temperatures of PAN (280-320 °C) is lower than PVP (343-361 °C). This means the PAN core would decompose earlier than the PVP shell when the temperature increased from room temperature to 280-320 °C. The releasing gas during the decomposition of the carrier polymer (polyacrylonitrile, PAN) driving the SnO₂ nanoparticles to the inwall of the PVP/FeCl₃ shell. As PVP exists in two mesomeric forms and there are strong interactions between the PVP and the metal oxide colloid (mainly H bonding), the nanoparticles could connect with each other even after the polymer was removed through high temperature sintering. Thus, the PVP shell and the interface PAN played a role as template for the final structure of α -Fe₂O₃/SnO₂ composite nanofibers. When the annealing temperature was final up to 700 °C, the SnO₂ and Fe₂O₃ nanoparticles constituted the internal and external of the product, respectively. To investigate how the morphology and structure of the material changing with the calcination conditions, we have conducted two group experiments with different calcined temperatures and heating rates as shown in Fig.S4 (details in ESI†).

X-Ray diffraction (XRD) analysis was performed to confirm the crystallization of the SnO₂/Fe₂O₃ nanofibers. The typical XRD pattern is shown in Fig.2 a, from which the crystal phase of the product was the mixed oxide of SnO₂ and α -Fe₂O₃. Most of the diffraction peaks could be indexed to the tetragonal structure of SnO₂, which agreed well with the reported values from the Joint Committee on Power Diffraction Standards card (JCPDS, 77-452). The residual peaks are well indexed to the rhombohedral

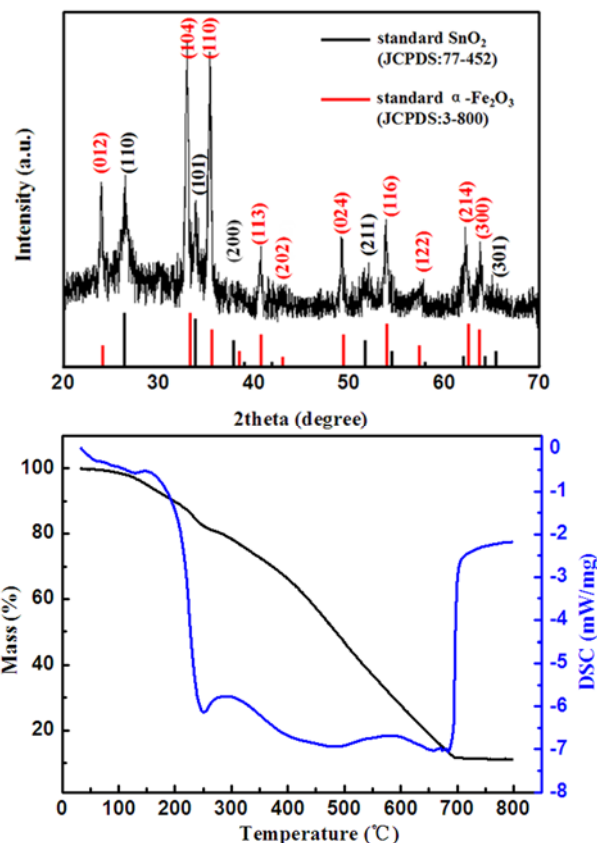


Fig. 2 (a) XRD pattern of the as-prepared composite nanofibers, (b) TG and DSC curves of the precursor

structure of α -Fe₂O₃, which are consistent with the standard date file 3-800. The result demonstrates the product as a mixture of SnO₂ and α -Fe₂O₃. No other diffraction peaks corresponding to impurities are observed, which indicate that the product has a high purity. Fig. 2 b shows the TG-DSC analysis of the precursor nanofibers. The first loss peak on the TG curve appears before 200 °C (endothermic DSC peak at 150 °C), which can be ascribed to the degradation of the side chain of the polymer (PAN and PVP). The following loss between 250 and 400 °C (predominantly exothermic DSC peak at around 250 °C) is attributed to the decomposition of FeCl₃ and SnCl₄ and the main chain of the polymer (PAN and PVP). Furthermore, the weight loss between 400 and 700 °C is due to the complete decomposition of the polymer (PAN and PVP) and FeCl₃ to α -Fe₂O₃ phase, SnCl₄ to SnO₂ phase. The DSC curve between 400 and 700 °C showing no obvious endothermic or exothermic peak also evidences the transition of precursor from amorphous to crystalline phase. When the temperature is higher than 700 °C, no weight loss is observed, indicating the complete transformation from precursor to α -Fe₂O₃/SnO₂ composite nanofibers.

Fig 3a shows the response plot of the sensor toward 100 ppm acetone as a function of operating temperature. The response increases with the operating temperature and reaches its maximum value of 5.3 at 275 °C, and then decreases with a further increase of temperature. Fig. 3b displays the response of sensor to 100 ppm acetone at 275 °C. The response time defines the time taken for the sensor to achieve 90% of the total resistance, and the recovery time is the time for the resistance recovery to 90% of the initial level after removal of acetone vapor. The response curve shows a drastic decline once the sensor is exposed to target gases and achieves a near steady state then rises to its initial value in air. The response and recovery times of the

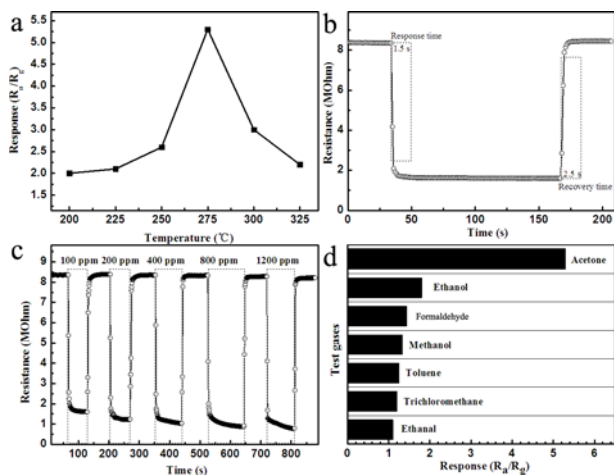


Fig. 3 (a) Response of sensor based on $\alpha\text{-Fe}_2\text{O}_3/\text{SnO}_2$ composite to 100 ppm acetone as a function of operating temperature. The gas response of sensor is defined as the ratio of the resistance of the sensor in air (R_a) to that in tested gases (R_g). (b) Response transients of the sensor to 100 ppm acetone at 275 °C. (c) Response transients of the sensor to different concentration of acetone at 275 °C. (d) Cross-responses of the sensor to various test gases (100 ppm concentration) at 275 °C.

sensor are about 1.5 and 2.5 s. The rapid response and recovery properties can be attributed to the novel cage-like construction, which provides excellent channel structure and more active sites accelerating the chemical absorption and stripping of the gas. The response and recovery behaviors were further investigated with the sensor being orderly exposed to different concentrations of acetone from 100 to 1200 ppm at an operating temperature of 275 °C. The result is displayed in Fig. 3 c. The response and recovery characteristics are almost reproducible with the quick time of response and recovery in Fig 3 c. As shown in Fig. 3 d, when the operating temperature reaches 275 °C, the sensor exhibits an excellent selectivity to acetone among the tested gases (ethanol, trichloromethane, toluene, methanol, formaldehyde, ethanol and acetone). The selectivity of sensor may be influenced by the reactive energy of test gases, operating temperature of sensor, and catalytic effect of $\alpha\text{-Fe}_2\text{O}_3/\text{SnO}_2$.²⁶ Different gases possess different energies to adsorption and desorption on the surface of sensing material. At lower temperature, the response is restricted by the speed of chemical reaction, and at high temperature, by the speed of diffusion of gas molecules. At some intermediate temperature, the speeds of two processes become equal, and at that temperature, the sensor response reaches to its maximum.²⁷ Moreover, the reaction between acetone and adsorbed oxygen will be accelerated by the catalytic effect of $\alpha\text{-Fe}_2\text{O}_3/\text{SnO}_2$, which leads to the high response to acetone.

In conclusion, a simple electrospinning method was used to prepare $\alpha\text{-Fe}_2\text{O}_3/\text{SnO}_2$ composite nanofibers. As a proof-of-concept demonstration of the function, such $\alpha\text{-Fe}_2\text{O}_3/\text{SnO}_2$ composite material was used as the sensing material of gas sensor. An enhanced sensing property to acetone was demonstrated with a short response and recovery times (1.5 and 2.5 s) to 100 ppm acetone at 275 °C. This result certainly provides the way to develop high performance sensors by electrospinning, which can be extended to the rest of the active materials and it also has an actual application prospect.

This work was supported by NSFC (61134010, 61327804, 61304242, 61374218) and Program for Chang Jiang Scholars and

Innovative Research Team in University (No. IRT13018), National High-Tech Research and Development Program of China (863 Program, No. 2013AA030902) and the project development plan of science and technology of Jilin Province (20130521009JH).

Notes and references

1. M. Ding, D. C. Sorescu and A. Star, *Journal of the American Chemical Society*, 2013, **135**, 9015-9022.
2. P. Sun, X. He, W. Wang, J. Ma, Y. Sun and G. Lu, *CrystEngComm*, 2012, **14**, 2229-2234.
3. P. Sun, Y. Liu, X. Li, Y. Sun, X. Liang, F. Liu and G. Lu, *RSC Advances*, 2012, **2**, 9824-9829.
4. P. Sun, Z. Zhu, P. Zhao, X. Liang, Y. Sun, F. Liu and G. Lu, *CrystEngComm*, 2012, **14**, 8335-8337.
5. P. Sun, X. Mei, Y. Cai, J. Ma, Y. Sun, X. Liang, F. Liu and G. Lu, *Sensors and Actuators B: Chemical*, 2013, **187**, 301-307.
6. Y. Guan, C. Wang, B. Wang, J. Ma, X.-m. Xu, Y.-f. Sun, F.-m. Liu, X.-s. Liang, Y. Gao and G.-y. Lu, *Chem. Res. Chin. Univ.*, 2013, **29**, 837-840.
7. X. Zhou, C. Wang, W. Feng, P. Sun, X. Li and G. Lu, *Materials Letters*, 2014, **120**, 5-8.
8. P. Sun, X. Zhou, C. Wang, K. Shimanoe, G. Lu and N. Yamazoe, *Journal of Materials Chemistry A*, 2014, **2**, 1302-1308.
9. Y. Guan, D. Wang, X. Zhou, P. Sun, H. Wang, J. Ma and G. Lu, *Sensors and Actuators B: Chemical*, 2014, **191**, 45-52.
10. P. Sun, C. Wang, X. Zhou, P. Cheng, K. Shimanoe, G. Lu and N. Yamazoe, *Sensors and Actuators B: Chemical*, 2014, **193**, 616-622.
11. D. D. Vuong, K. Q. Trung, N. H. Hung, N. V. Hieu and N. D. Chien, *Journal of Alloys and Compounds*, 2014, **599**, 195-201.
12. P. Sun, Y. Cai, S. Du, X. Xu, L. You, J. Ma, F. Liu, X. Liang, Y. Sun and G. Lu, *Sensors and Actuators B: Chemical*, 2013, **182**, 336-343.
13. C. Zhu, Y. Li, Q. Su, B. Lu, J. Pan, J. Zhang, E. Xie and W. Lan, *Journal of Alloys and Compounds*, 2013, **575**, 333-338.
14. B. B. Wang, X. X. Fu, F. Liu, S. L. Shi, J. P. Cheng and X. B. Zhang, *Journal of Alloys and Compounds*, 2014, **587**, 82-89.
15. N. Yamazoe, K. Suematsu and K. Shimanoe, *Sensors and Actuators B: Chemical*, 2012, **163**, 128-135.
16. N. Yamazoe, K. Suematsu and K. Shimanoe, *Thin Solid Films*, 2013, **548**, 695-702.
17. M.-H. Seo, M. Yuasa, T. Kida, J.-S. Huh, N. Yamazoe and K. Shimanoe, *Sensors and Actuators B: Chemical*, 2011, **154**, 251-256.
18. Z. Wang, H. Yin, C. Jiang, M. Safdar and J. He, *Applied Physics Letters*, 2012, **101**, 253109.
19. X. Sun, H. Ji, X. Li, S. Cai and C. Zheng, *Journal of Alloys and Compounds*, 2014, **600**, 111-117.
20. J. Song, M. Chen, M. B. Olesen, C. Wang, R. Havelund, Q. Li, E. Xie, R. Yang, P. Bøggild and C. Wang, *Nanoscale*, 2011, **3**, 4966-4971.
21. X. Cao, C. Xu, Y. Liu and Y. Chen, *Carbohydrate polymers*, 2013, **92**, 69-76.
22. A. Yarin, *Polymers for Advanced Technologies*, 2011, **22**, 310-317.
23. Z. Kurban, A. Lovell, S. M. Bennington, D. W. Jenkins, K. R. Ryan, M. O. Jones, N. T. Skipper and W. I. David, *The Journal of Physical Chemistry C*, 2010, **114**, 21201-21213.
24. L. Xu, R. Zheng, S. Liu, J. Song, J. Chen, B. Dong and H. Song, *Inorganic chemistry*, 2012, **51**, 7733-7740.
25. Z. Zhang, X. Li, C. Wang, L. Wei, Y. Liu and C. Shao, *The Journal of Physical Chemistry C*, 2009, **113**, 19397-19403.
26. M. Rumyantseva, V. Kovalenko, A. Gaskov, E. Makshina, V. Yuschenko, I. Ivanova, A. Ponzoni, G. Faglia and E. Comini, *Sensors and Actuators B: Chemical*, 2006, **118**, 208-214.
27. N. J. Dayan, S. R. Sainkar, R. N. Karekar and R. C. Aiyer, *Thin Solid Films*, 1998, **325**, 254-258.